

**PARAMETRIC AND EXPERIMENTAL ANALYSIS  
USING A  
POWER FLOW APPROACH**

**J.M. Cuschieri  
Center for Acoustics and Vibration  
Department of Ocean Engineering  
Florida Atlantic University  
Boca Raton, Florida 33431.**

**February 1988**

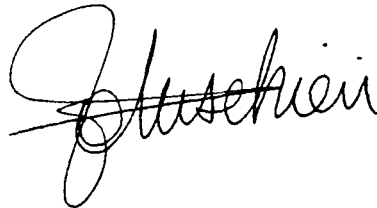
**Third Semi-annual Report  
Grant Number NAG-1-685**

**Submitted to  
National Aeronautics and Space Administration  
Langley Research Center  
Hampton VA 23665**

FORWARD

This report describes the work performed during the first half of the second year of the research project under Research Contract NAG-1-685, entitled "Use of Energy Accountancy and Power Flow Techniques for Aircraft Noise Transmission". The author would like to acknowledge the financial support by NASA Langley through the Acoustics Division. Also special thanks to the graduate assistants who worked on this project and to the department of Ocean engineering at Florida Atlantic University.

Submitted by  
J.M. Cuschieri  
Principal Investigator

A handwritten signature in cursive script, appearing to read "J. Cuschieri", written in dark ink.

# ABSTRACT

Having defined and developed a structural power flow approach for the analysis of structure-borne transmission of structural vibrations, the technique is used to perform an analysis of the influence of structural parameters on the transmitted energy. As a base for comparison the parametric analysis is first performed using a Statistical Energy Analysis approach and the results compared with the results obtained using the power flow approach. The advantages of using structural power flow are thus demonstrated by comparing the type of results that are obtained by the two methods. Additionally, to demonstrate the advantages of using the power flow method and to show that the power flow results represent a direct physical parameter that can be measured on a typical structure, an experimental investigation of structural power flow is also presented. In this experimental investigation results are presented for an L-shaped beam for which an analytical solution has already been obtained. Furthermore, the various methods available to measure vibrational power flow are compared to investigate the advantages and disadvantages of each method.

## SECTION I

### INTRODUCTION

Power flow analysis for the evaluation of the vibration response of coupled structures was developed for two coupled structures [1, 2]. In one case the coupled structure consists of an L-shaped beam pinned at the junction. This represents a one-dimensional flow of the vibrational power and the coupling between the structure was a point contact. Although the analytical analysis of this coupled structure was of a somewhat simple nature, it demonstrated the application of the power flow technique. Also the analytical results obtained from this study served as a tool for the evaluation of experimental power flow results for a finite structure.

The second case represents the analysis of a coupled two-dimensional structure in the form of an L-shaped plate. In this analysis the power flow concept, where the flow of vibrational power is expressed in terms of mobility functions, was extended to deal with two-dimensional (line) joints. This required the use of mobility functions defined not only as functions of frequency but also as functions of space. The total flow of vibrational power from one plate substructure to another is obtained through an integral over the entire length of the joint.

In both cases the results obtained using the power flow technique were compared to results obtained using Finite Element Analysis (FEA) and Statistical Energy Analysis (SEA). The purpose of this comparison is twofold. First it demonstrated that the power flow method can be a useful tool in the mid frequency range. For the structure used in the previous analysis the mid frequency region was in the range of 100 Hz to 1 KHz. In this frequency region FEA starts to break down unless the mesh used in the modeling of the structure is close enough to resolve the short wavelengths, while SEA produced only general levels which can be significantly different from the actual response levels. The second purpose was to check the accuracy of the results as compared to these other types of analysis in those frequency regions where FEA and SEA are known to be accurate. Comparison with FEA at low frequencies showed very good agreement between the results both in terms of levels and the locations of the resonant modes of the global structure. This was an interesting result because in the evaluation of the mobility functions only the uncoupled modes of the substructures were identified, but when the coupling equations, in terms of the mobility functions of the substructures at the joint and at the point of excitation were implemented, both the coupled and uncoupled modes were generated in the results and the number of modes was identical to the number of modes obtained from the FEA modeling. The comparison of results at high frequencies with

results from SEA also show good agreement and indeed show that when consecutive structural modes start to couple the fluctuations in the response of the structure are reduced and the response approaches a mean level similar to the level predicted by SEA.

Having shown the development of the power flow technique especially for the two-dimensional (line) joint case, and its comparison for accuracy with other well established techniques, the next objective is to show the additional modal information that is obtained in determining the response of a substructural component using power flow techniques due to changes in the structural parameters of the source and receiver substructures.

Comparison with FEA in this case is somewhat of a limited value because in using FEA, given enough computing power and the generation of a fine mesh for the structure model, accurate detailed modal results can be obtained. However the computing power required may be prohibitive and the generation of the mesh needs to be very accurate. In this case comparison of computational efficiency may be more appropriate. Power flow is more efficient computationally because the global structure is divided into substructural components and the analysis performed on the individual substructures, which are then joined together through the mobility expressions. These mobility expressions once derived hold for any combination of coupled substructures and it's a matter of adding the required number of terms for all the substructures and the joints.

FEA can also be used on the substructures to evaluate the required mobility functions. In this application since each substructure is analyzed independently of the rest of the global structure, a much finer mesh can be used to generate accurate results up to higher frequencies. Because of the smaller size of the structure, a finer mesh will still be within the limits of the computational hardware that is used for the analysis. An additional advantage of the substructuring is that common substructures can have their mobility functions stored in a database, very much similar to structure elements in a finite element package, which would then make the approach even more efficient. Furthermore, the results obtained using power flow, since these can be obtained for selected joints of the global structure representing the flow of vibrational power through that joint, have a more useful physical meaning in vibration analysis as compared to the overall deflections and stresses as one would normally obtain using FEA. This power flow through the joint represents all the vibrational power that is either radiated, dissipated by the structure or distributed to other joined substructures.

Comparing power flow results to SEA results, the advantages in using power flow in the medium frequencies can be better

demonstrated. This comparison is to some extent more important because in this case, SEA is significantly more efficient computationally and thus the requirement and indeed availability of detailed modal response information obtained by using a power flow approach needs to be well established.

In performing these comparisons with SEA, the next section in this report, presents results for the power ratio and energy level of the receiver substructure for the case of two coupled substructures obtained using an SEA approach. Also investigated is the change in power ratio due to structural modifications and how these compare to the similar results obtained using a power flow approach. The parametric analysis using the power flow method is not complete, but the results obtained thus far already show some of the advantages of power flow over SEA in the mid frequencies.

In Section IV, the experimental results for the power flow measurements of the L-shaped beam are presented. These results demonstrate the type of information that can be obtained experimentally and how this ties with the analytical results. In this section one can get an understanding of the type of physical results that can be obtained using the power flow approach. Also in this section is a discussion on the available techniques that can be used for the measurement of power flow and the significance and errors associated with each technique.

## SECTION II

### STATISTICAL ENERGY ANALYSIS

An SEA approach is used to study the influence of different structural parameters on the energy levels and transmission of vibrational power for an L-shaped plate. Where applicable the results in this section are interpreted in a graphical form as presented by Maidanik [3] which summarizes the influence of structural parameters in terms of the changes in the coupling and dissipation loss factors. The net power transmitted from the source plate to the receiver plate is equal to the power dissipated by the receiver plate since no external sources of power or other receivers of vibration are attached to the receiver plate. The only connection to the receiver plate is the source plate. In this analysis only bending waves are considered, the contributions from longitudinal and transverse waves is negligible.

#### II.1. Power Ratio And Energy Levels

The power ratio  $R$ , ratio of the transmitted power to the input power, can be expressed as a function of  $\eta_{12}/\eta_1$  (ratio of the power flowing from the source plate to the receiver plate to the power dissipated in the source plate) and  $\eta_{21}/\eta_2$  (ratio of the power flowing from the receiver plate to the source plate to the power dissipated in the receiver plate) [3].

$$R = \frac{\eta_{12}/\eta_1}{\eta_{12}/\eta_1 + \eta_{21}/\eta_2 + 1} \quad (1)$$

$\eta_{ij}$  represent coupling loss factors between substructures  $i$  and  $j$  and these are functions of the substructure parameters.  $\eta_i$  represent dissipation loss factors.

It is convenient to represent  $R$  on a parametric plane defined by  $\eta_{12}/\eta_1$  and  $\eta_{21}/\eta_2$  (figure 1) [3]. The parametric state of the system is designated by a point in the positive quadrant of the parametric plane, since loss factors are always positive. A constant value of the power ratio is represented by a straight line where the slope represents the value of  $R$ . The slope decreases with increasing  $R$  value. The influence of a change in  $\eta_1$ ,  $\eta_2$ ,  $\eta_{12}$  or  $\eta_{21}$  on the value of  $R$  can thus be deduced from such a diagram.

It can be observed that the power ratio decreases with decreasing  $\eta_{12}/\eta_1$  ratio (path 2, figure 1) and increases with the  $\eta_{21}/\eta_2$  ratio (path 1). However  $\eta_{12}$  and  $\eta_{21}$  are not independent but are related by the expression

$$n_1 \eta_{12} = n_2 \eta_{21} \quad (2)$$

where  $n_1$  and  $n_2$  are the modal densities of the source and receiver plates respectively. Increasing the isolation between the two systems (that is, decreasing  $\eta_{21}$  and  $\eta_{12}$ ) can result in only small variations in the power ratio, since the two effects cancel out.

Rewriting R in another form:

$$R = \frac{1}{1 + (n_1 \eta_1) / (n_2 \eta_2) + \eta_1 / \eta_{21}} \quad (3)$$

In some frequency regions,  $\eta_{21} \gg \eta_1$  (figure 2) and thus R mainly depends on the ratio  $\eta_1 / \eta_2$ . And therefore in this case, the power ratio can only be changed by modifying the damping of the plates, while the isolation has no significant effect. As the frequency increases,  $\eta_{21} / \eta_1$  becomes more significant, and thus if  $\eta_1 / \eta_2$  is kept constant, variations in  $\eta_1$  or  $\eta_{21}$  will result in significant changes on the power ratio.

The energy level of the receiver plate  $E_2$  can be expressed as

$$E_2 = \frac{\Pi R}{\omega \eta_2} = \frac{\Pi}{\omega} \frac{1}{\eta_2 + (n_1 \eta_2 / n_2) + (\eta_2 \eta_1 / \eta_{21})} \quad (4)$$

where  $\Pi$  represents the power input to the source plate. With changes in the coupling loss factors,  $E_2$  varies in the same way as R. However,  $E_2$  and R behave differently when the damping loss factors are changed. If  $\eta_2$  increases, then  $E_2$  decreases whereas R increases. Since at low frequencies  $\eta_1 \ll \eta_{21}$ , and  $\eta_2 \ll \eta_{21}$ , R and  $E_2$  can only be reduced by increasing  $\eta_1$ .

The above discussion dealt with the variation in the energy level and the power ratio in general terms, where coupling loss factors and dissipation loss factors were considered. In what follows, the specific influence of different plate parameters which control the coupling loss factors and the dissipation loss factors will be investigated. The size, thickness and material of the plates will influence the coupling loss factors, whereas the structural damping influences the dissipation loss factors.

## II.2. Influence Of Plates' Sizes

The influence of the plates' sizes is demonstrated by computing the power ratio for different ratios of the receiver plate area ( $S_2$ ) to the source plate area ( $S_1$ ). The coupling loss factors  $\eta_{12}$  and  $\eta_{21}$  are inversely proportional to the



area  $S_1$  of plate (i). If the area ratio  $S_2/S_1$  increases, the value of  $R$  increases (path 1 in figure 1). For a given input power to the source plate, the receiver plate can dissipate more power ( $\eta_2$  constant) and therefore the transmitted power increases (figure 3). The increase in the power ratio decreases as the value of  $S_2/S_1$  increases. This can be explained by the fact that the transmitted power asymptotically approaches the input power as the area ratio increases. For the source plate much larger than the receiver plate any increase in area ratio results in a large increase in the power ratio.

### II.3. Influence Of Plates' Thicknesses

To study the influence of the plates' thicknesses, the power ratio is determined as a function of the ratio of the source plate thickness ( $H_1$ ) to the receiver plate thickness ( $H_2$ ). In this case the power ratio has a maximum value for plate thickness ratios of between 1 and 2. The thickness ratio for which  $R$  is a maximum tends to unity as the frequency increases (figure 4). This peak in the power ratio can be explained by considering the influence on the coupling loss factors when the thickness ratio changes.  $\eta_{12}$  and  $\eta_{21}$  do not exhibit identical behavior (figure 5). For low values of  $H_2/H_1$  both  $\eta_{12}$  and  $\eta_{21}$  increase by approximately the same rate with increasing thickness ratio,  $\eta_{21}$  is however greater than  $\eta_{12}$  (point 1 figure 6). As  $H_2/H_1$  approaches unity  $\eta_{21}$  starts to decrease (point 2 to point 3 figure 6) and eventually at  $H_2/H_1 = 1$ ,  $\eta_{21} = \eta_{12}$  (point 4). Beyond this point both  $\eta_{21}$  and  $\eta_{12}$  decrease but this time  $\eta_{12} > \eta_{21}$  and thus the power ratio starts to decrease again (point 5).

An additional feature of the power ratio curve as a function of thickness ratio is that for a given frequency, the curve is asymmetric. The power ratio decreases at a faster rate for thickness ratios greater than 1 than it does for a thickness ratio smaller than 1. This can be explained using a wave model. For  $H_2/H_1 < 1$  all the incident waves on the junction have a component which is partially transmitted. However for  $H_2/H_1 > 1$  incident waves at an angle greater than a critical angle [5] are completely reflected, that is there is no transmitted component and therefore less power flows through the joint.

The thickness ratio has a greater influence on the power ratio than does the area ratio. For a given reduction of weight obtained either by a variation of thickness or a variation of area, the reduction in the power ratio is greater in the first case. A variation of area has an influence on the levels of energy in the plates whereas a variation of thickness has also an influence on the way the energy is transmitted through the junction.

#### II.4. Influence Of Plate Material

The power ratio is practically independent of material differences except under such conditions where the bulk wave speed of the two materials is significantly different. For two identical plates but of different materials the difference in the power ratio is less than 1 dB (figure 7). For materials with the same bulk wave speed such as aluminium and steel, the coupling loss factors  $\eta_{12}$  and  $\eta_{21}$  are not influenced by the change of the material and thus the power ratio is not modified.

#### II.5. Influence Of Structural damping

The structural damping will influence the dissipation loss factors. Two conditions are considered to investigate the influence of the dissipation loss factor on the power ratio and the level of energy of the receiver plate.

##### II.5.1. Plates with equal structural damping

For two identically damped plates, a significant reduction in the power ratio is obtained with increasing structural damping (path 4 in figure 1). As the damping increases more energy is dissipated in the source plate and less power is available for transmission to the receiver plate. This result is however strongly dependent on the frequency. At low frequencies changes in the dissipation loss factor are somewhat masked by the high coupling loss factor. At high frequencies significant reductions in the power ratio are obtained with changes in the dissipation loss factor (figure 8). At high frequencies the coupling loss factors are reduced, hence the dependency on the dissipation loss factor increases. With regards to the energy level of the receiver plate, this is significantly reduced with increasing dissipation loss factor (figure 9).

##### II.5.2. Plates with different structural damping

A significant reduction of power ratio is observed for two plates with different dissipation loss factors, especially if the damping of the source plate is higher than that of the receiver plate (path 2 on figure 1). The power ratio is strongly controlled by the structural damping of the source plate rather than by the structural damping of the receiver plate. This is an expected result since from equation (2),  $\eta_1$  is present in two of the terms of the denominator. Because the transmitted power is taken to be equal to the power dissipated by the receiver plate, the power ratio increases with increasing dissipation loss factor of the receiver plate (figure 10).

The results for the energy level of the receiver plate are however different in this case as compared with the case of equal damping. From equation (3),  $\eta_2$  and  $\eta_1$  play symmetrical roles

for two plates with identical modal densities ( $n_1 = n_2$ ). Thus an important factor is the relative magnitudes of the dissipation loss factors to the coupling loss factors. In general for most of the frequency range  $\eta_{12}$  and  $\eta_{21}$  are greater than .05 (figure 2) and the energy level of the receiver plate is lower when the coupling loss factors are of the same order of magnitude as the dissipation loss factors. This is in comparison with the dissipation loss factor being much lower than the coupling loss factor. When the dissipation loss factors are much smaller (.001 or .01) than the coupling loss factors, there is no significant influence on the energy level of the receiver plate (figure 11).

### SECTION III

#### STRUCTURAL POWER FLOW

Having obtained the dependency of the ratio of transmitted power to input power on the various structural parameters associated with an L-shaped plate using SEA, in this section similar results will be obtained using a power flow technique. The results obtained in this section will be compared to the results in section II. With the structural power flow approach [1,2] the transmitted power or power ratio is obtained from input and transfer mobility functions at the location of excitation and the joint, and between these two locations respectively. The dependency of the transmitted power on the structural parameters using a power flow approach is not yet fully completed. Thus in what follows in this section is a presentation of the results obtained thus far, which do not include analysis on the influence of plates sizes, thicknesses and materials. Work is still in progress on the influence of these structural parameters. An additional analysis is however presented on the influence of the excitation location on the level of transmitted power. This type of information is completely unavailable using SEA.

##### III.1. Influence of Plate Damping

The case that is considered here is for both plates having the same level of structural damping. Given a constant level of excitation at a fixed location (the location considered is off the center of the source plate) the input and transmitted power and the power ratio are evaluated (figure 12 (a,b,c)). It can be observed from these figures that the power flow has a strong dependency on the dissipation loss factor only for high loss factor values and at high frequencies.

This result is in full agreement with the results obtained using an SEA approach (figure 8) where the reduction in power ratio is only significant at high frequencies and for dissipation loss factors higher than 0.01. Comparing the two sets of results (figures 8 and 12(c)) the agreement is also very good in terms of the power ratio levels. However comparing the results for the transmitted power using the power flow approach (figure 12(b)) to the results for the energy level of the receiver plate (figure 9) the two sets of results are different, especially in the conclusions that can be made. The reason for this is that although both of these results represent power or energy of the receiver plate the two energy/power terms are different although related. To obtain the transmitted power from the energy level, one must multiply the latter with frequency and overall loss factor, that is including power transmission to other substructures. In the case considered here the receiver plate is only connected to the source plate and thus the overall loss factor is the same as the dissipation loss factor. Thus the

energy level results (figure 9) when multiplied by  $2\pi$  frequency and  $\eta_2$  will give a level of approximately -4 dB. This level is based on an assumed power input of unity. Thus if one compares this with the power transfer curve (figure 12(b)) and takes into account that the power input is not unity but given by figure (12(a)), then the two results match in terms of mean levels.

Comparing the power flow results to the SEA results one can immediately observe the more detailed results obtained using the power flow method. In fact the transmitted power curve and the power ratio curve show some interesting features, especially for low dissipation loss factors. The ratio of transmitted power to input power as computed using the power flow approach has fluctuations of up to 10 dB about the mean level estimated using SEA. However the value computed by the power flow approach at the natural frequencies of the global structure match exactly with the levels estimated using SEA. Thus, while at the resonances the SEA results are accurate (same as power flow), off resonances large discrepancies can be obtained between actual results and SEA results. Because at some frequencies the power ratio off resonances is much higher than the mean level predicted with SEA, the results from the power flow approach can be significant in predicting the power transfer due to forced motion off resonances. As damping increases, the discrepancy between the power flow results and the SEA results is reduced and in fact the power flow results will approach the SEA results. This is expected from consideration of dissipation of the vibrational energy before it reaches the boundaries of the structure, thus no reflection from the boundaries would occur and a standing wave pattern is not set up.

### III.2. Influence of Excitation Location.

A set of results which cannot be obtained using an SEA approach is with regards to the influence of the excitation location on the transmitted and input vibrational power. Using the SEA approach, because of the spatial averaging, the results are for a generalized location of the excitation. However intuitively, the excitation location can be important and can reduce the input vibrational power if the input location can be controlled. To demonstrate this, results have been obtained for the L-shaped plate configuration for a set of excitation locations starting at the center of the plate. The results here can be extended to determine the optimum excitation location relative to the position of a rib in a stiffened structure.

Figures (13) and (14) show respectively the power input and output and the power ratio for excitation positions ranging from a location at 50% of the plate length perpendicular to the joint, to 4% of the same plate length away from the joint. As can be observed from these results while the ratio of transmitted to input power does not significantly change, the input power is

extensively reduced, on the order of about 20 dB reduction at the resonant peaks when the excitation position is moved from 50% to 4% of the plate length from the joint.

Although these type of results are mainly applicable to the situation where the excitation is well defined, as compared to distributed excitation, they demonstrate some of the advantages of using the power flow method.

Thus far these have been the two structural parameters that have been investigated. Work is still in progress to obtain the dependency on the other parameters discussed in section II.

## SECTION IV

### EXPERIMENTAL ANALYSIS

The vibrational power flow between two beams joined in an L-shaped configuration is investigated experimentally and the results compared to analytical results [1]. Another way to evaluate the transmitted power apart from the method presented in [2] is to express the power flow through a beam cross section i as follows:

$$P_1 = \langle M_1(t) \dot{\theta}_1(t) + F_1(t) V_1(t) \rangle \quad (1)$$

where  $P_1$  is the power flow,  $M_1(t)$  is the bending moment,  $\dot{\theta}_1(t)$  is the angular velocity,  $F_1(t)$  is the shear force, and  $V_1(t)$  is the transverse velocity. This technique to measure power flow was developed by Noiseux [6], and later further investigated by Redman-White [7] for infinite beam or beams with a low standing wave ratio (SWR). The L-shaped beam structure used in this present analysis has a high SWR and part of the study is to investigate different methods to measure the flow of vibrational power in the presence of strong non propagating (standing wave) components.

#### IV.1. Measurement Of Power Flow

From equation (1), the power-flow through a cross-section of the beam has contributions from two components, the shear force component  $P_s$ , which is given by the product of the shear force and the transverse velocity, and the bending moment component  $P_m$ , which is given by the product of the bending moment and the rotational velocity. Away from discontinuities, the time averaged values of  $P_s$  and  $P_m$  are equal [7], that is the transmitted power is shared equally between the shear force component and the bending moment component. Therefore, the power flow can be approximated by twice the shear force component, as long as the cross-section of interest is away from structural discontinuities. That is;

$$P_1 = 2 \langle P_s \rangle \quad (2)$$

The advantage of this simplification is that the total transmitted power can be related to the first and lower order space derivatives which would simplify the required measurements. Expressing the shear force component of the power flow in terms of the displacement  $w(x,t)$  of the beam

$$P_s = E I \partial^3 w / \partial x^3 \partial w / \partial t \quad (3)$$

where E is the Young's modulus and I is the second moment of area.

The third order derivative in equation (3) can be expressed in terms of a product of a first order derivative of the displacement and the bending wavenumber and frequency [7].

$$P_m = E I (-k^2 \partial w / \partial x) (\partial w / \partial t) \quad (4)$$

Since accelerations  $a(x,t)$  are generally measured in an experiment, it is useful to modify  $P_m$  in terms of acceleration rather than displacement

$$P_m = \sqrt{(\rho A E I) / (2\pi f)^2} \langle \partial a(t) / \partial x a_q(t) \rangle \quad (5)$$

where the subscript q indicates "in quadrature"

Equation (5) can be evaluated using either of two different methods. Pavic [8] suggests the use of a "direct" method, where time domain processing is implemented to get the time-averaged value of power, while Verheij [9] proposes a cross-spectral density method which for a particular frequency f gives

$$P_m(f) = \sqrt{(\rho A E I) / (8\pi^2 f^2)} \text{Real} \{ \partial a(f) / \partial x j a^*(f) \} \quad (6)$$

The pros and the cons of these two methods have been discussed by Verheij [9] and Pavic [10] but only in terms of the development of practical instrumentation for field measurements. That is, there is a lack of comparison of results obtained by either of these two approaches. In this paper the two techniques are applied on the L-shaped beam structure.

The data required in equations (5) and (6) can be obtained by using finite difference approximations and the signals obtained from two linear accelerometers spaced a small distance  $\Delta$  apart [7]. The two acceleration terms in equations (5) and (6) can then be expressed in terms of  $a_1, a_2$  where  $a_1$  and  $a_2$  represent the acceleration measurements at the two closely spaced positions respectively. That is

$$a = (a_1 + a_2) / 2 \quad \partial a / \partial x = (a_2 - a_1) / \Delta \quad (7)$$

and equation (5) becomes



$$P_m = \sqrt{(\rho AEI)/(8\pi^2 f^2 \Delta)} \langle a_1 a_{2q} - a_2 a_{1q} \rangle \quad (8)$$

since  $\langle a_1 a_{2q} \rangle - \langle a_2 a_{1q} \rangle$  is equal to zero [7].

Alternatively from equation (6)

$$P_m = \sqrt{(\rho AEI)/(2\pi^2 f^2 \Delta)} \text{Imag}\{S[a_1(f), a_2(f)]\} \quad (9)$$

where  $S$  is the cross-spectral density function between the two acceleration measurements.

#### IV.2. Theoretical Analysis

The close-form solution developed in [1] was used to compute the theoretical power flow vectors at locations along the two sections of the L-shaped beam. Most of the power is transmitted at the resonant frequencies and the reason for this is that maximum energy dissipation occur when the amplitude of vibration is high. These frequencies have therefore been selected for the measurement of the power flow. Figure (15) shows a plot of the propagating vibrational power level from the excitation point to the end of the receiver beam. Three curves are plotted: the exact result given by equation (1), the results obtained after the approximation that the power flow is equal to twice its shear force power component is implemented (equation (3)) and finally the results obtained after finite difference approximation is implemented (equation 8). It can be observed from the exact results that the power flow decreases steadily to reach zero at the end of the receiver beam. Since these are theoretical results, the joint does not have any influence on the power flow when obtained using the exact solution.

The results obtained using equation (7) are in good agreement with the results from the exact solution away from discontinuities. That is near the beam ends and near the joint, discrepancies exist between the two results. The approximate expression underestimates the power flow level near the joint. Most of the power close to this discontinuity is propagated by the bending moment component and the shear force component is very small. This result is also a consequence of the condition that the joint is pinned, that is no displacement is allowed but only rotation. On the other hand, the power flow is overestimated near the free ends of the beams. In this case, most of the power is propagated by the shear force component whereas the bending moment component is much smaller. The effects of the nearfield of a discontinuity, that is the length of beam for which  $P_m$  and  $P_m$  are not equal is a function of frequency since it is related

to the wavelength. The higher the frequency, the smaller the length of the beam for which discrepancies occur.

Another observation that can be made is that the level of power flow decreases for increased frequencies. This is in agreement with the calculations for the total transmitted power.

The error introduced by the finite difference approximation is very much dependent on the spacing  $\Delta$  of the accelerometers. If the value of  $\Delta$  is increased to obtain a better signal-to-noise ratio and signal phase discrimination, the error associated with the finite difference approximation increases. A trade-off is found between these two conflicting requirements by selecting a spacing of the order of 15% of the wavelength of the highest frequency of interest [7]. For such a  $\Delta$ , it can be shown that the error introduced due to the finite difference approximation is acceptable.

#### IV.3. Experimental Set-up

The experimental set-up consists of two identical steel beams of thickness  $3/8"$  (0.9525 Cm), width  $3"$  (7.62 Cm) and length  $36"$  (91.44 Cm). The beams are welded to a  $5/8"$  diameter steel rod such that they form a ninety degrees angle at the joint. The rod provides a means of pinning the joint so that the experimental set-up matches the boundary conditions imposed in the theoretical analysis. The rod is held by two flange bearings mounted on a base structure. The harmonic excitation is provided by means of an electromagnetic shaker threaded into the source beam and supported by a heavily damped brace. It should be noted that the bearing assembly was found to have a great effect on the vibration level of the beam. When the two bearing braces were lightly forced apart, the vibration level decreased significantly. A schematic of the experimental set up including the processing layout is shown in figure (16).

#### IV.4. Experimental Power Flow Measurements

The power flow was measured using two Bruel&Kjaer 4375 accelerometers and the signal processing performed on an HP5451C analyzer. From equations (8) and (9), the power flow is highly dependent on the difference in phase between the two accelerometer locations. Hence, it is necessary to calibrate the entire instrumentation chain. That is, the accelerometers, the charge amplifiers and the data processing system including all connections. For this purpose, the accelerometers were subjected to an identical linear acceleration and the phase difference evaluated. The set-up used for the calibration is shown in figure (17) which is identical to the one used in [7]. The length of the bar was chosen to insure that the first longitudinal frequency was much higher than the maximum frequency of interest. From these calibration results the measured phase difference was of

the order of 0.5 degree. The gain difference was found to be less than one per cent. In the power flow experiment proper spacing of the accelerometers was insured by using a placing jib.

#### IV.4.1 Time Domain Method

Using equation (8) and the processing procedure shown in figure (18), that is all the processing done in the time domain except for the introduction of the phase quadrature, a measure of the transmitted power is evaluated. The time-average of the final signal was obtained from the amplitude of the Fourier Transform of the acceleration at the frequency of excitation. Single frequency excitation at a selected resonance of the combined structure was used with the process repeated for each frequency of interest.

The power flow results for the beams with an average loss factor of 0.015 are shown in figure (19) for five different frequencies. There are some discrepancies in the results since it would be expected that power flows away from the input location to the remote end of the structure. To try to find the reason for the errors in these results, the sensitivity of the difference in phase between the two input signals to the data processing routines was investigated. Two signals with a known phase difference were processed and the actual phase difference compared with that given at the result of the processing. The results are shown in Table I. It can be observed that an error of about 5% is obtained for a phase difference of ninety degrees but the error increases as the phase angles decrease, with up to 25% error for phase differences less than five degrees. An increase of the number of data points per sampling period did not improve the results.

It can therefore be concluded that processing errors can be significant for small phase angles which would explain the erroneous results obtained at low frequencies and towards the remote end of the beam, away from the excitation point where the power flow component is extremely low. Time domain processing would probably give better results if analogue processing is used instead of digital processing as was used by Redman-White [7] and Pavic [8].

#### IV.4.2. Frequency Domain Method

Using the processing procedure shown in figure (20) to implement equation (9), a measure of the power flow was obtained by taking the imaginary part of the cross spectrum at the frequency of excitation. The number of operations on the data in this case is smaller than with the time domain method. Fourier transforms are only used once instead of three times as in the time domain method. Single frequency excitation, at the resonant frequencies of the combined structure were used for the analysis.

The results for the beams with an average loss factor of 0.015 are shown in figure (21) and are consistent with expected results, especially for the source beam. Nevertheless, the power-flow is very small in the receiving beam which is a cause of error. For all frequencies except 256 Hz, the power-flow direction for the receiver beam close to the joint is in the direction of the joint. This is due to errors introduced very close to the joint discontinuity.

Figure (22) shows the results of the power flow measurements for the beams with an average loss factor of 0.054. These results show good agreement with theoretical results except that they are somewhat lower. This is due to slight discrepancies observed between the measured response level and the theoretical response level. This discrepancy was significant at low frequencies. In fact the agreement between experimental and analytical power flow results is better at high frequencies than at low frequencies. For the high frequencies, the power-flow in the receiver beam near the joint does not point towards it anymore, which supports the explanation that the reverse flow of power is caused by errors in the measurement of the very small phase angle differences.

Apart from single frequency excitation broad band excitation was also used to plot a map of power-flow for a wider range of frequencies. The results (figure 23) clearly show the decrease of power from the shaker to the end of the receiver beam, and also the increase in the level of power flow with frequency. When plotting these results on a log amplitude scale, these would be identical to the power flow as obtained analytically using the mobility expressions. The only differences in this case would be the discrepancies introduced due to the approximation of equation (2).

## SECTION V

### CONCLUSION

From the above analysis and results it can be concluded that the power flow method can be a very useful tool in the mid frequency range where the modal response of a structure is important. The type of results obtained, although limited to the type of structure being examined in this case, demonstrate that power flow is computationally efficient and can be used to deal with complex global structures. The technique is not limited to singly coupled plate like structures.

In the above analysis comparison has been made with results obtained using SEA, but these results were generated specifically for the purpose of comparison. In the literature one can find additional results that deal with singly coupled plates, such as the work by Boisson et al [11] for the evaluation of the energy level of coupled structures using an energy influence coefficient method. Similar results are obtained between SEA and the results by Boisson. The latter are one-third octave results which are therefore similar to SEA results. Additionally good agreement is obtained in the trends of the results for the influence of the excitation location on the transferred vibrational power between the power flow method and the energy influence coefficient method.

The state of knowledge in power flow is however still limited. Only point loading has been considered and in the application to aircraft structures it is equally important to consider distributed loading. Furthermore the extension to multiple substructures needs to be better, more fully defined. An example to demonstrate the application of the power flow approach to a set of repetitive structures joined together directly or through stiffeners, that is for a structure similar to an aircraft fuselage, needs to be developed. Extending this technique even further, one may want to investigate the modeling of composite structures, taking into account such additional structural parameters as the connection of fibers through joints and the influence of fiber orientation.

Finally as far as two dimensional structures are concerned detailed experimental analysis of the influence of structural parameters on the flow of vibrational power, which thus far has only been investigated analytically, needs to be performed. The experimental analysis should consist of both experiments on the structure similar to the one in the analytical model (L-shaped plate) but also on real aircraft structures in which case the conclusions derived from the analytical approach can be verified.

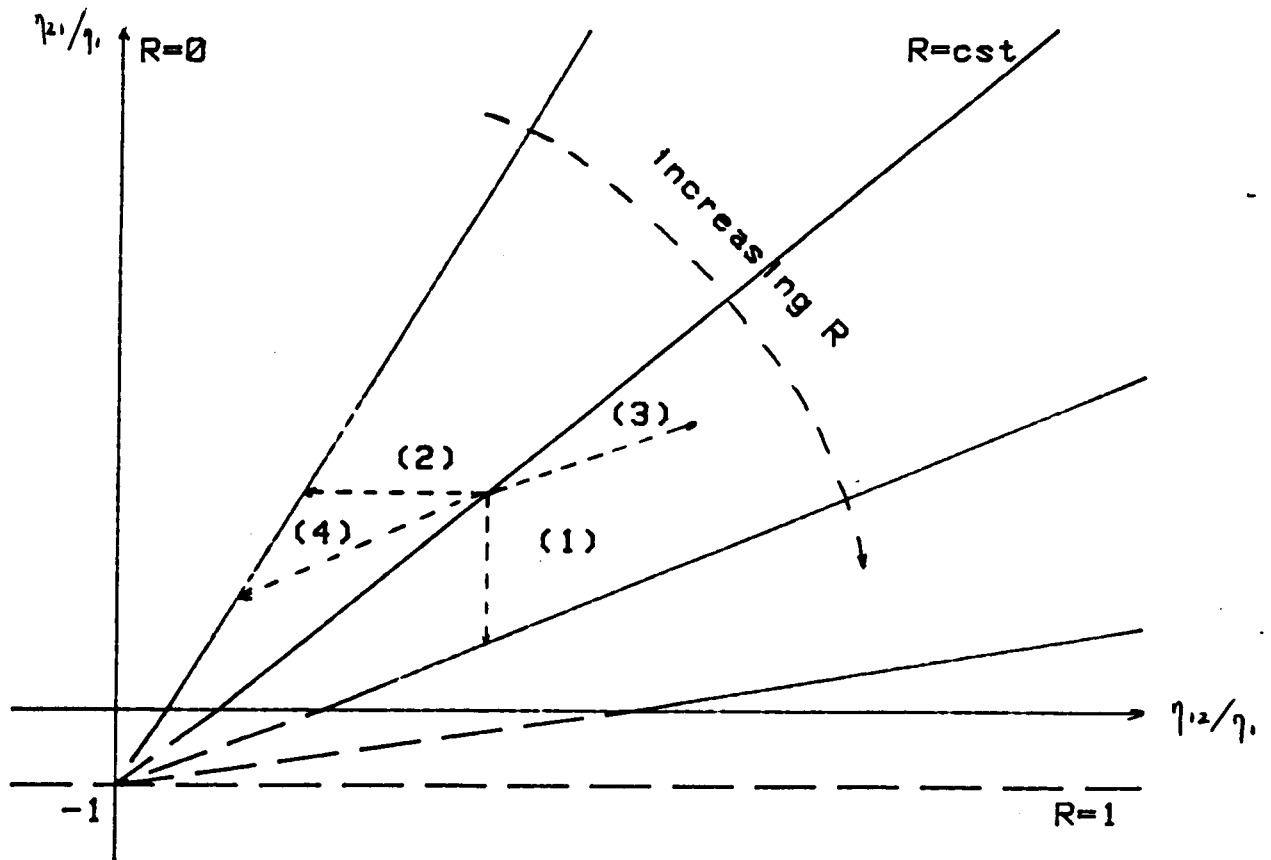
REFERENCES

1. J.M. Cuschieri "Power Flow as a Complement to SEA and Finite Element Analysis" ASME Publication NCA - Vol 3 (1987).
2. J.M. Cuschieri "Extension of Vibrational Power Flow Techniques to Two-dimensional Structures" First Annual Report Grant Number NAG-1-685 NASA Langley, Hampton VA. (1987).
3. G. Maidanik "Principle of Supplemantarity of Damping and Isolation in Noise Control" Journal of Sound and Vibration, 77(2), 245-250, (1981).
4. R.H. Lyon "In-plane Contribution to Structural Noise Transmission", Noise Control Engineering Journal 26(1), 22-27, (1986).
5. L. Cremer, M. Heckl, E.E. Ungar "Structure-borne Sound", Springer-Verlag, New York, 1973.
6. D.U. Noiseux "The Measurement of Structural Wave Intensity" Journal of the Acoustical Society of America, 47, 238-247, (1970).
7. W. Redman-White "The Measurement of Structural Wave Intensity " Ph. D. Thesis, University of Southampton, England, (1983).
8. G. Favic "Measurement of Structure-borne Wave Intensity" Journal of Sound and Vibration, 49, 221-230, (1976).
9. J.W. Verheij "Cross Spectral Density Methods for Measuring Structure Borne Power Flow on Beams and Pipes" Journal of Sound and Vibration, 70 133-139, (1980).
10. G. Favic, Response to a Letter to the Editor, Journal of Sound and Vibration, 70, 138-139, (1980).
11. C. Boisson, J.L. Guyader, P. Millot and C. Lesueur "Energy Transmission in Finite Coupled Plates, Part II: Application to an L Shaped Structure" Journal of Sound and Vibration, 81(1), 93-105, (1982).

TABLE I

Phase Difference Sensitivity on Calculated Power Flow

Actual Phase Difference	Measured Phase Difference	Error
90	69.7	6.2%
3.6	4.2	-23.2%
1.8	2.2	-26.1%



- (1)  $\eta_{21}/\eta_2$  decreasing i.e.  $\eta_2$  increasing
- (2)  $\eta_{12}/\eta_1$  decreasing i.e.  $\eta_1$  increasing
- (3)  $\eta_{12}/\eta_1$  and  $\eta_{21}/\eta_2$  increasing
- (4)  $\eta_{12}/\eta_1$  and  $\eta_{21}/\eta_2$  decreasing

FIGURE 1 : Parametric Representation of the Power Ratio



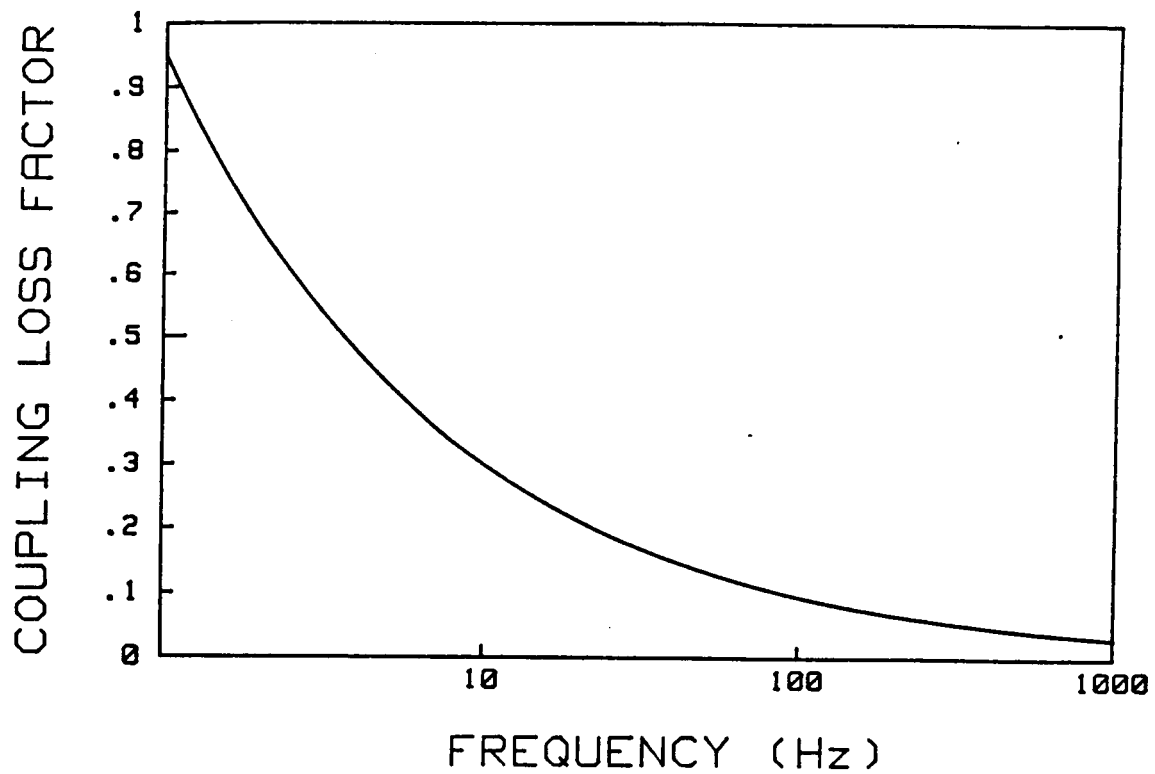


FIGURE 2. Coupling Loss Factors (  $\eta_{12}$  )  
for Plates of Equal Thickness

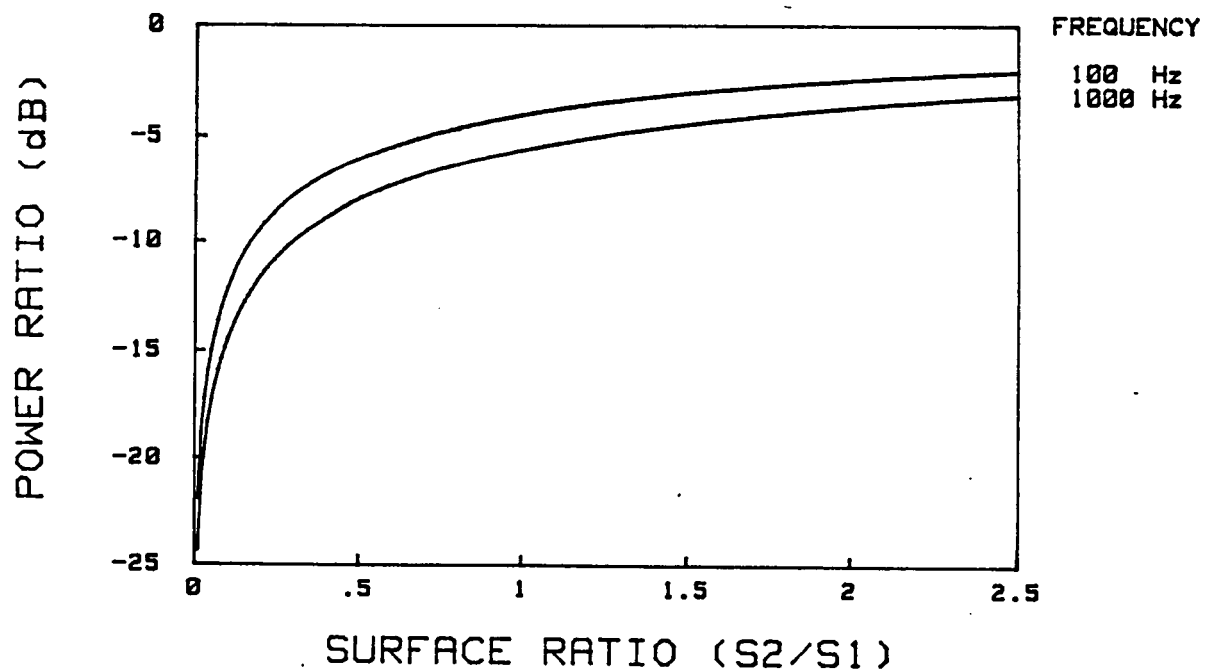


FIGURE 3. Power Ratio as a Function of the Area Ratio  
of the Two Plates

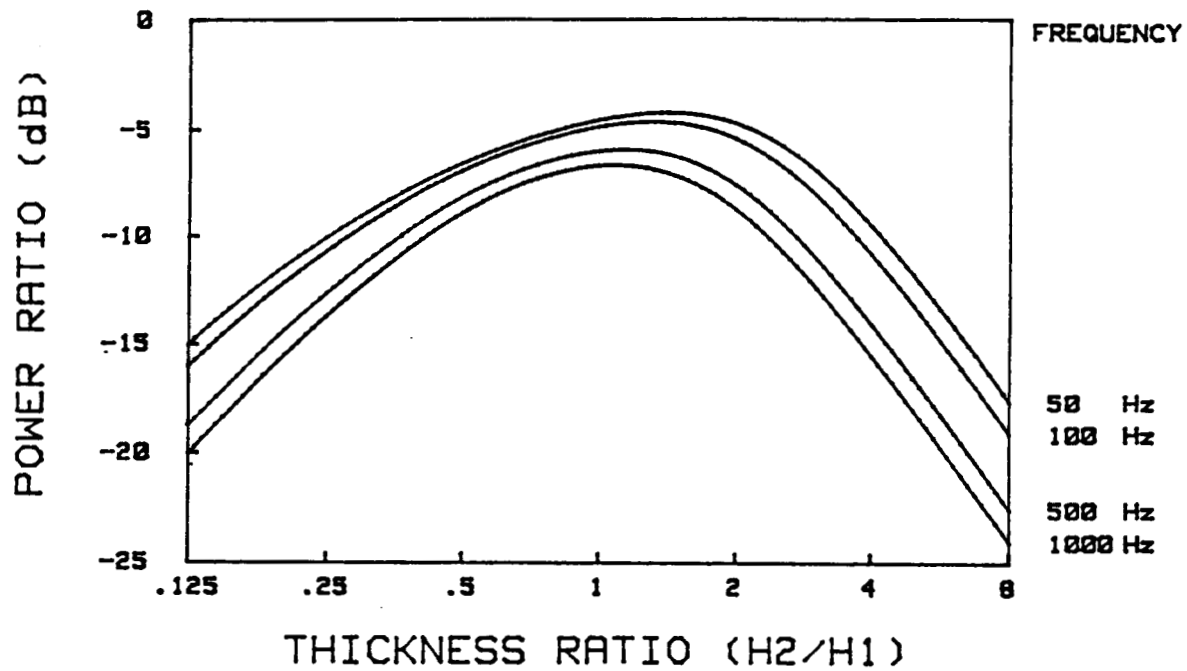


FIGURE 4. Power Ratio as a Function of the Thickness Ratio of the Two Plates

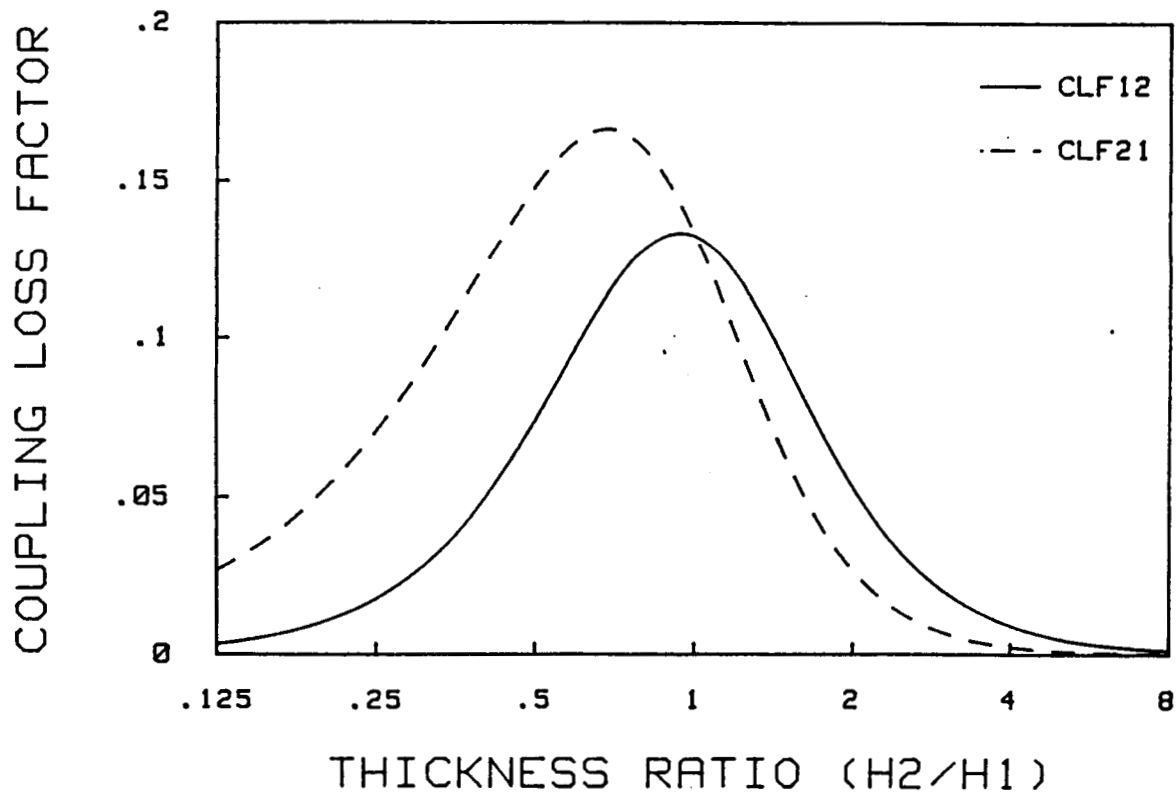


FIGURE 5. Coupling Loss Factors as Functions of the Thickness Ratio of the Two Plates, (frequency 500 Hz).

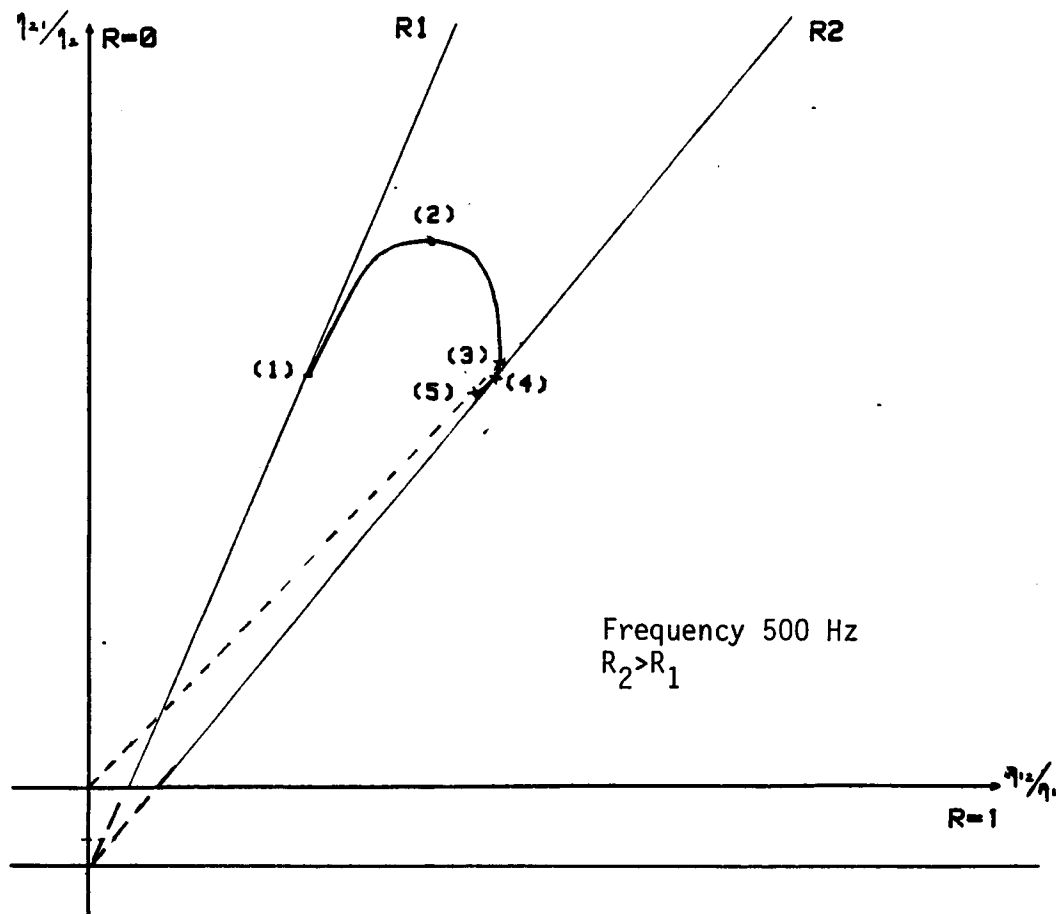


FIGURE 6. Parametric Representation of the Power Ratio as a Function of the Thickness Ratio

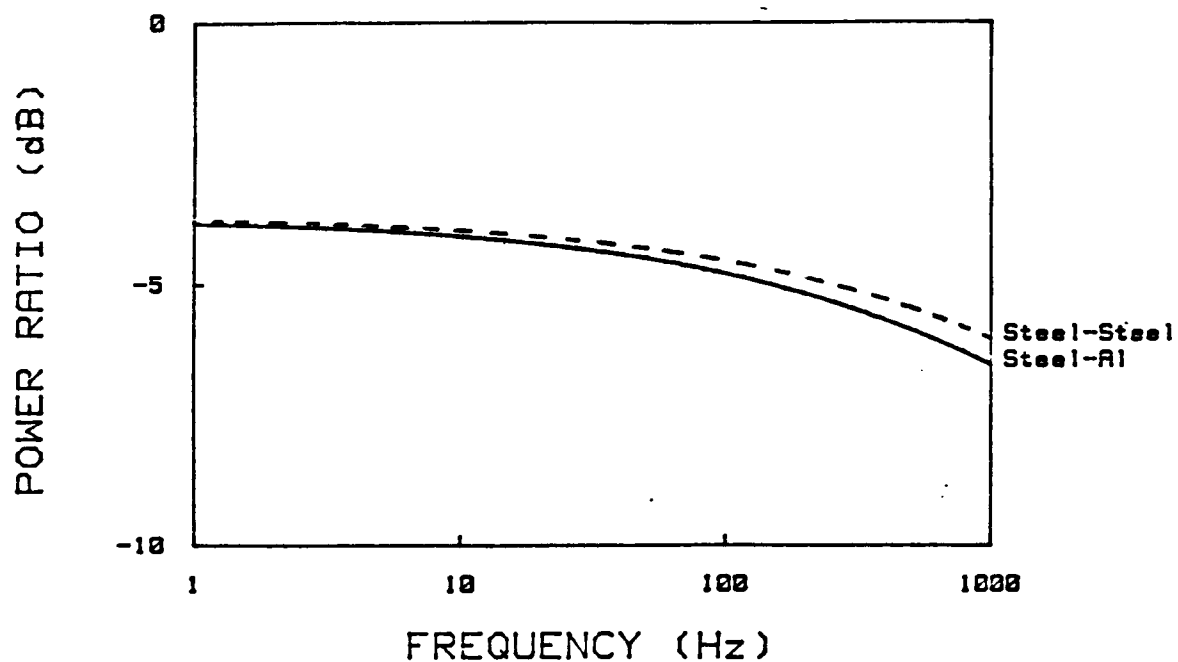


FIGURE 7. Power Ratio as a Function of the Plate Material

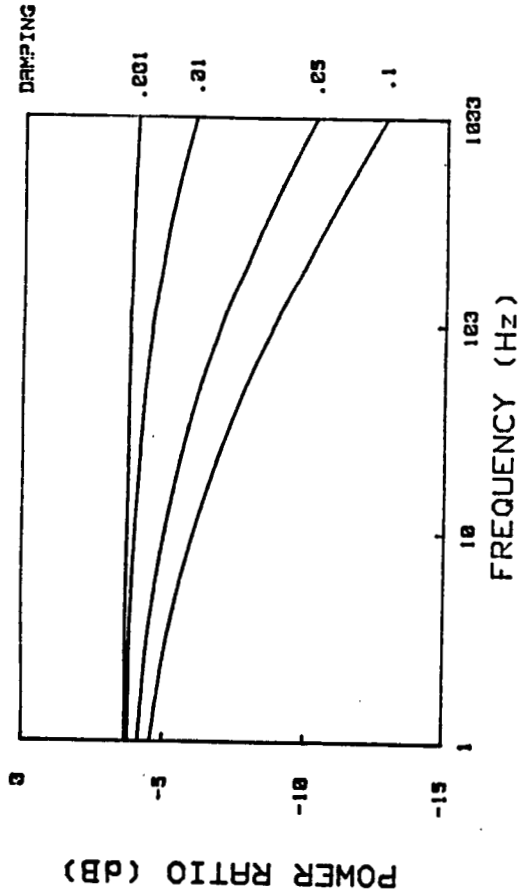


FIGURE 8. Power Ratio as a Function of Damping  
(Plates with equal damping).

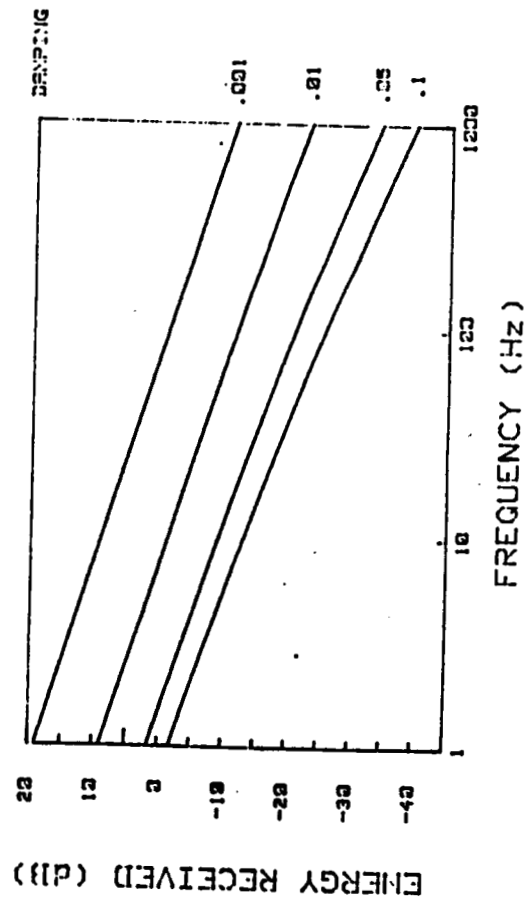


FIGURE 9. Energy of the Receiver Plate as a Function of Damping  
(plates with equal damping).

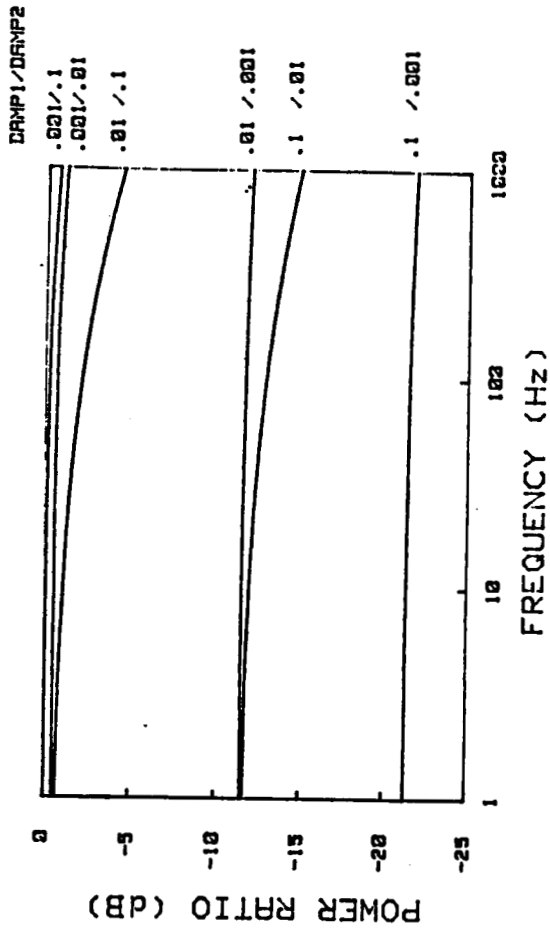


FIGURE 10. Power Ratio as a Function of Damping  
(plates with different damping).

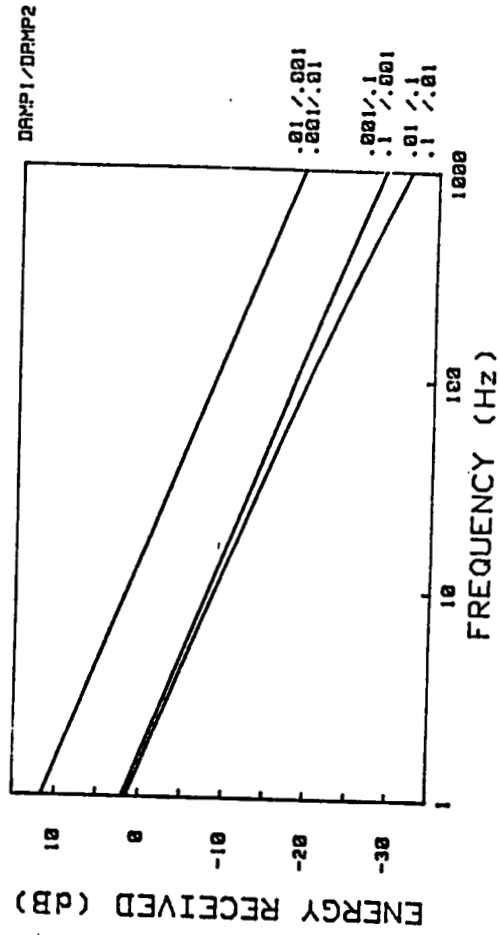


FIGURE 11. Energy of The Receiver Plate  
as a Function of Damping  
(plates with different damping).

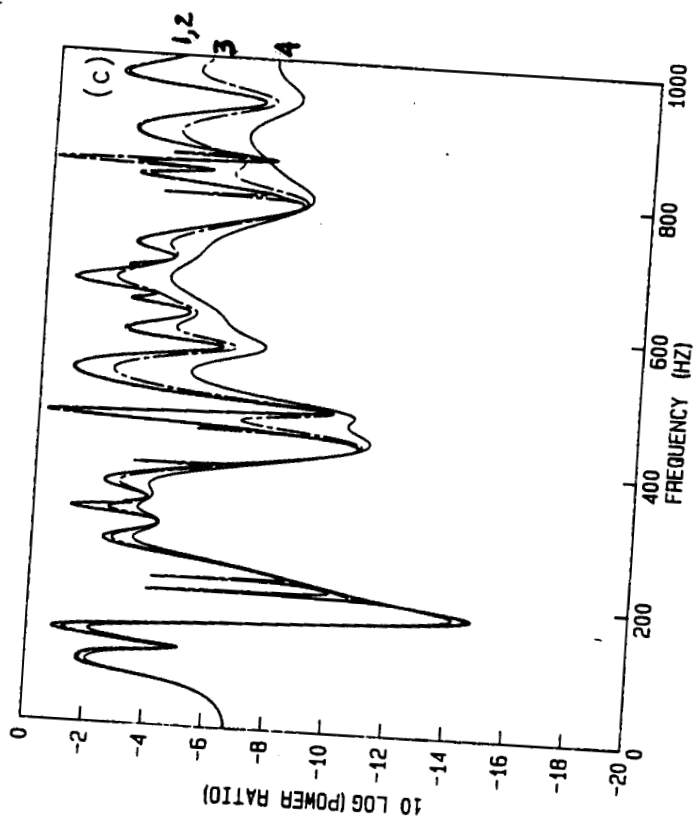
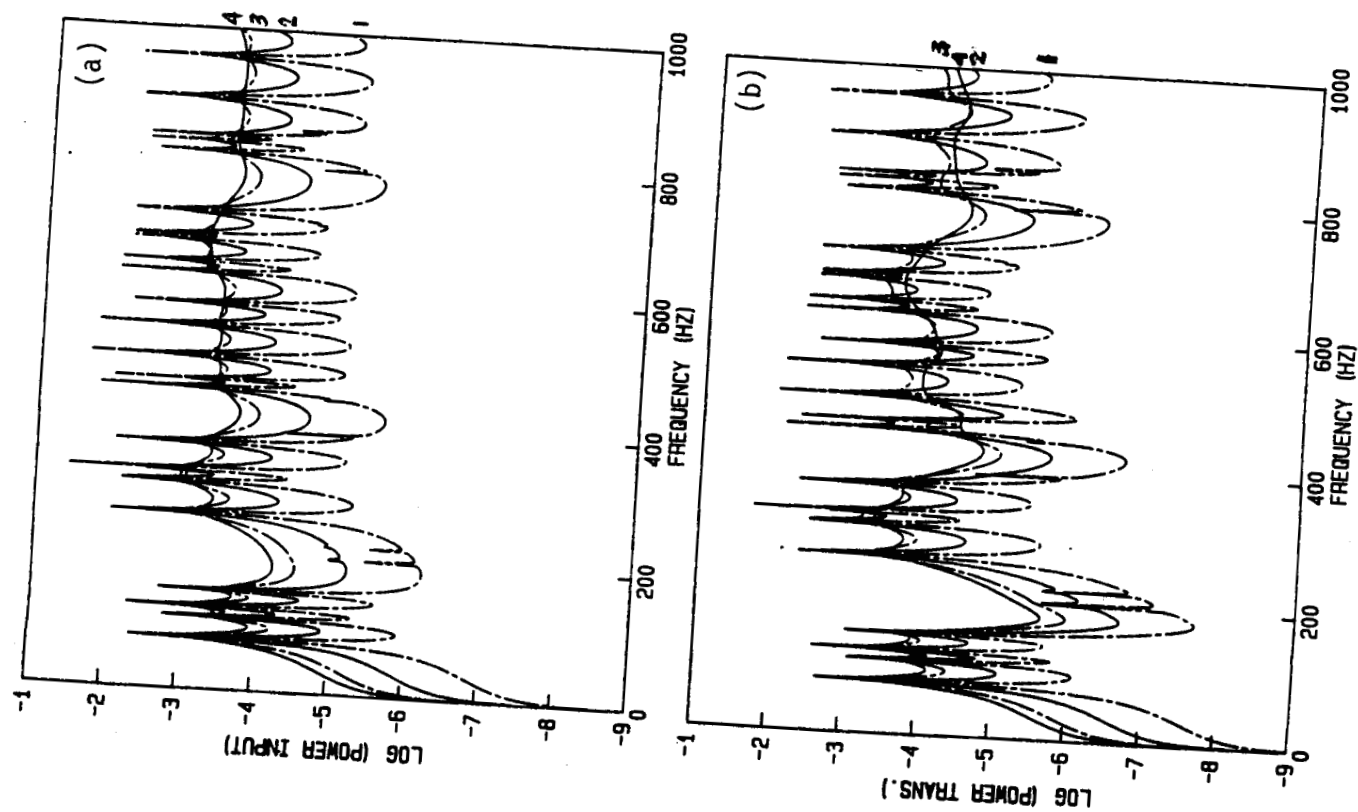


Figure 12. Power flow results as a function of structural loss factor for plates with equal damping and for plates with off center excitation.  
 (a) Power input per unit excitation force;  
 (b) power transfer per unit excitation force;  
 (c) power ratio. (1)  $\eta = 0.001$ ; (2)  $\eta = 0.01$ ; (3)  $\eta = 0.05$ ; (4)  $\eta = 0.1$

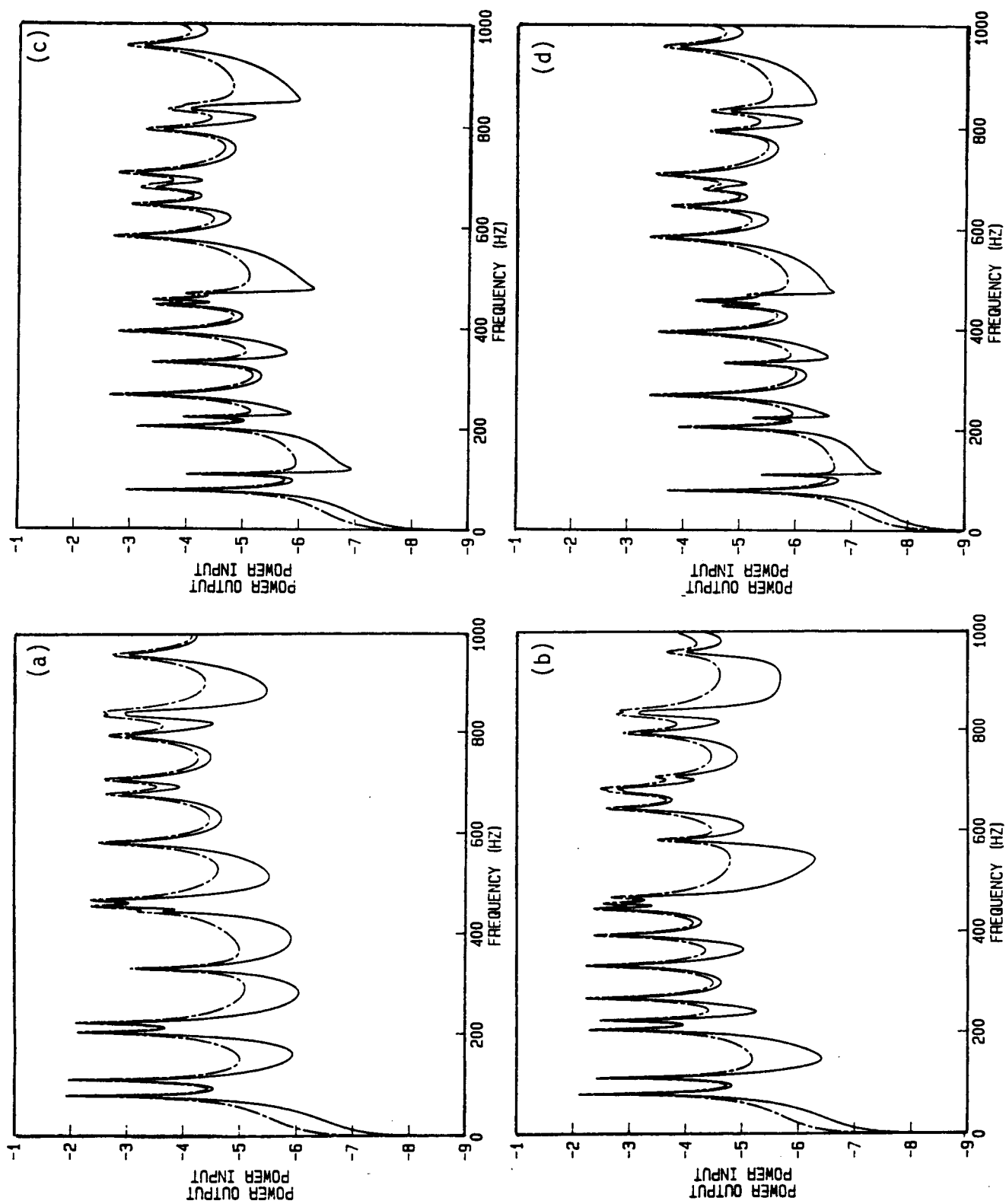


Figure 13. Power flow as a function of excitation location. (a) 50%; (b) 30%; (c) 10%; (d) 4% of plate length away from joint.

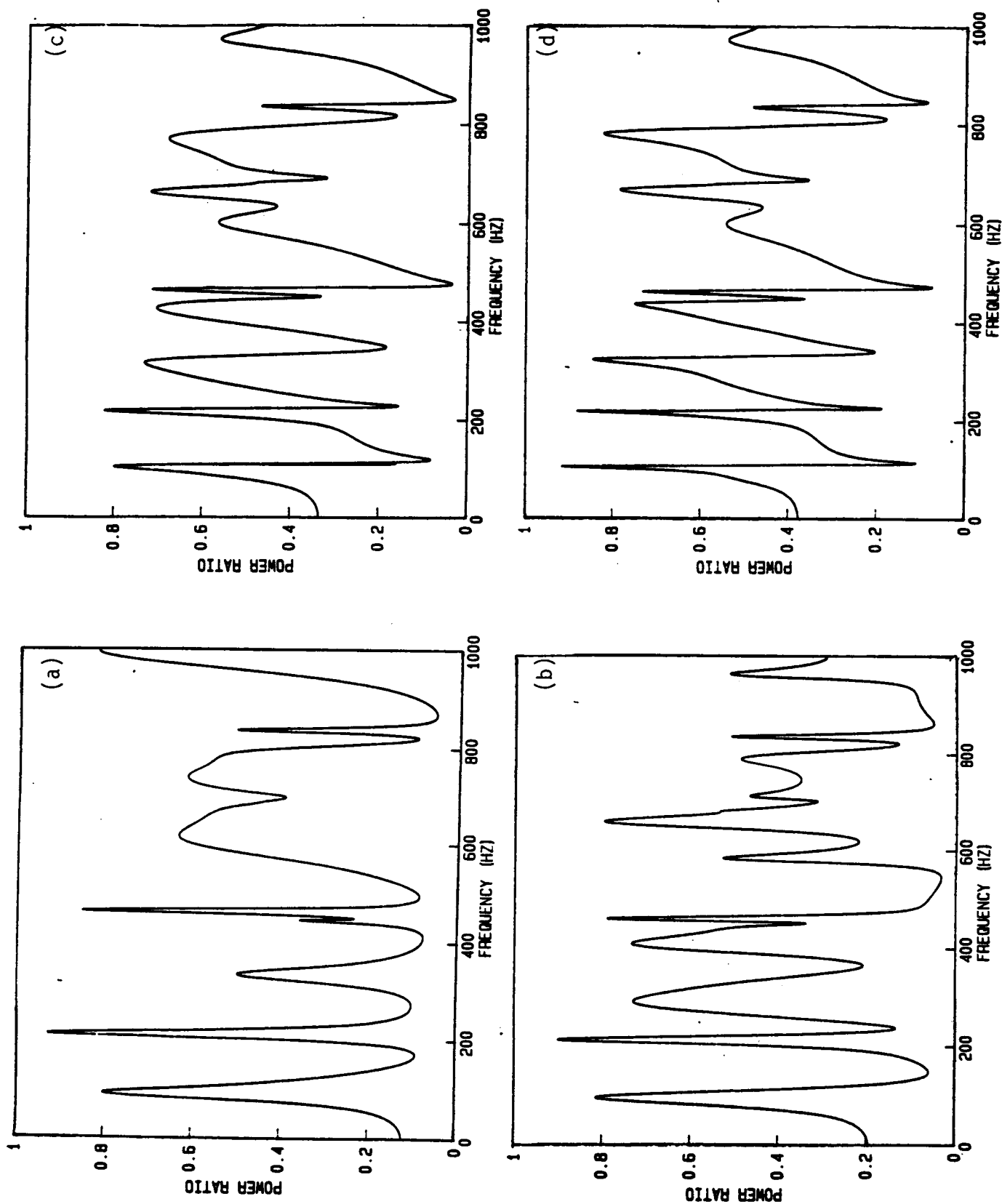


Figure 14. Power flow results for power ratio as a function of excitation location. (a) 50% ; (b) 30% ; (c) 10% ; (d) 4% of plate length away from joint.

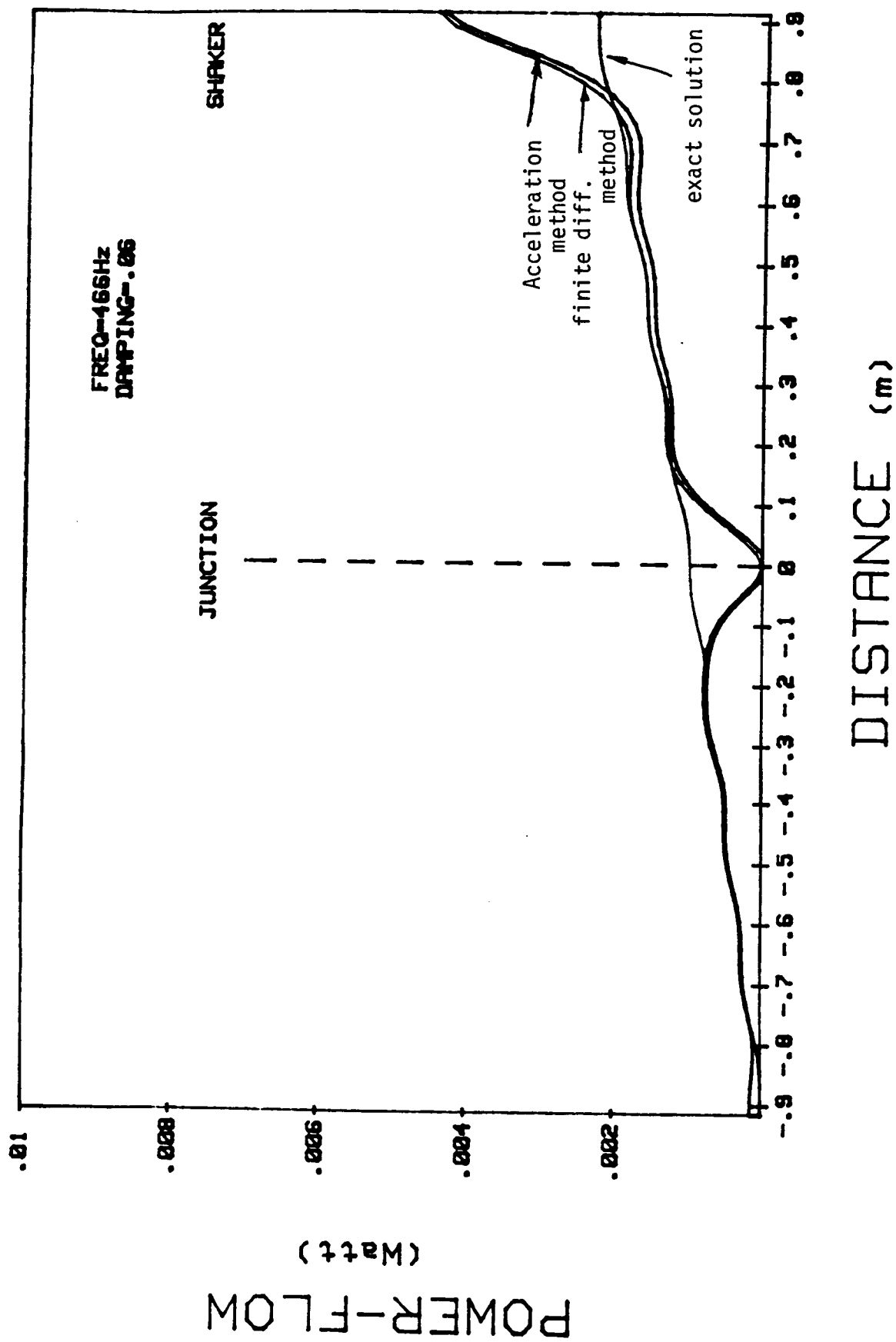


Figure 15. Power Flow in L-shaped beam, exact and approximated results



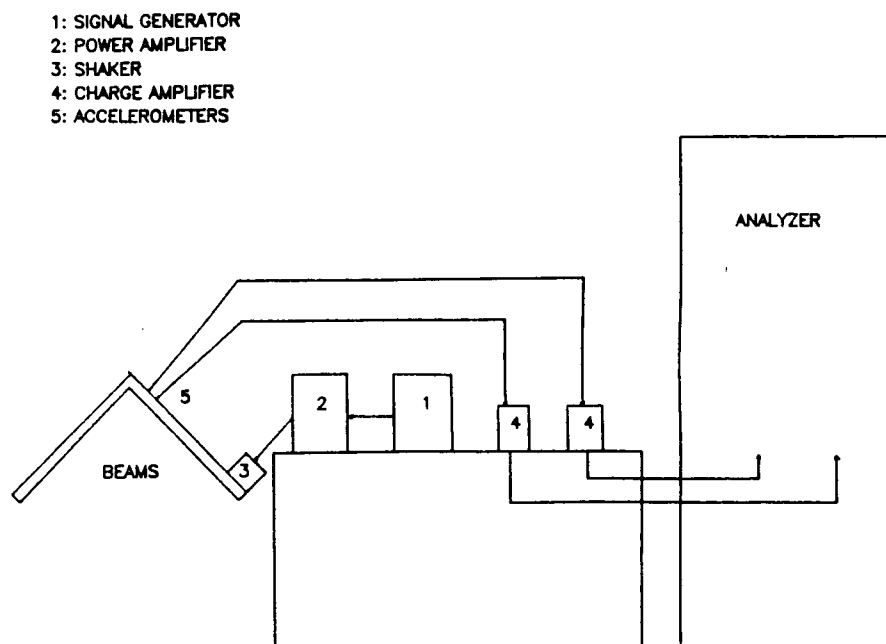


Figure 16. Schematic representation of experimental set up for the measurement of power flow.

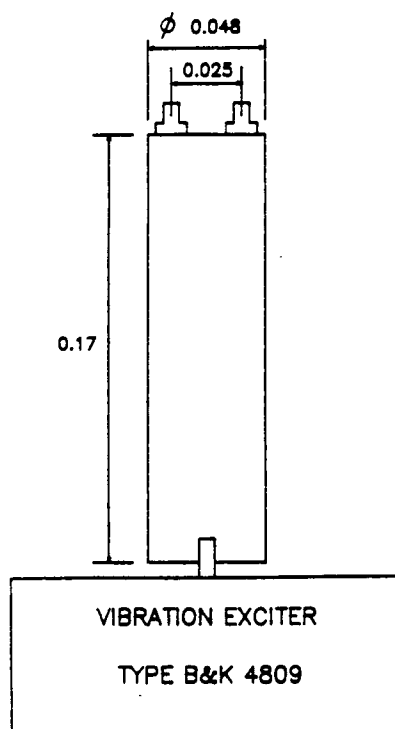


Figure 17. Set up for the phase calibration of the measurement system.

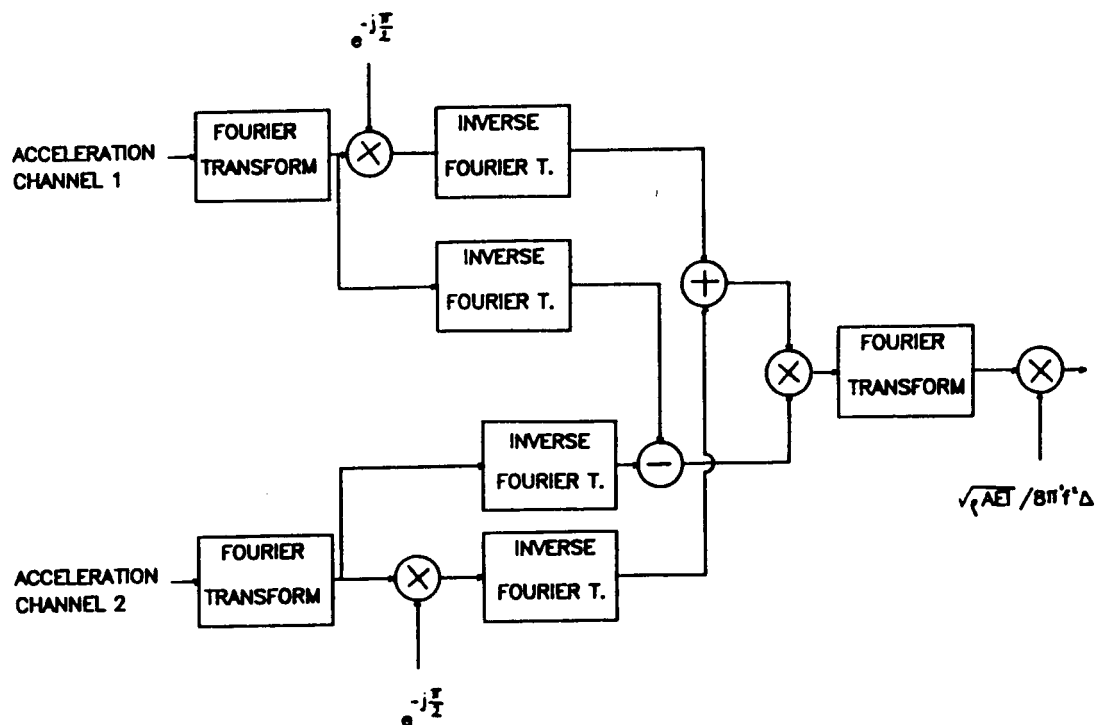


Figure 18. Processing procedure for the time domain evaluation of power flow.

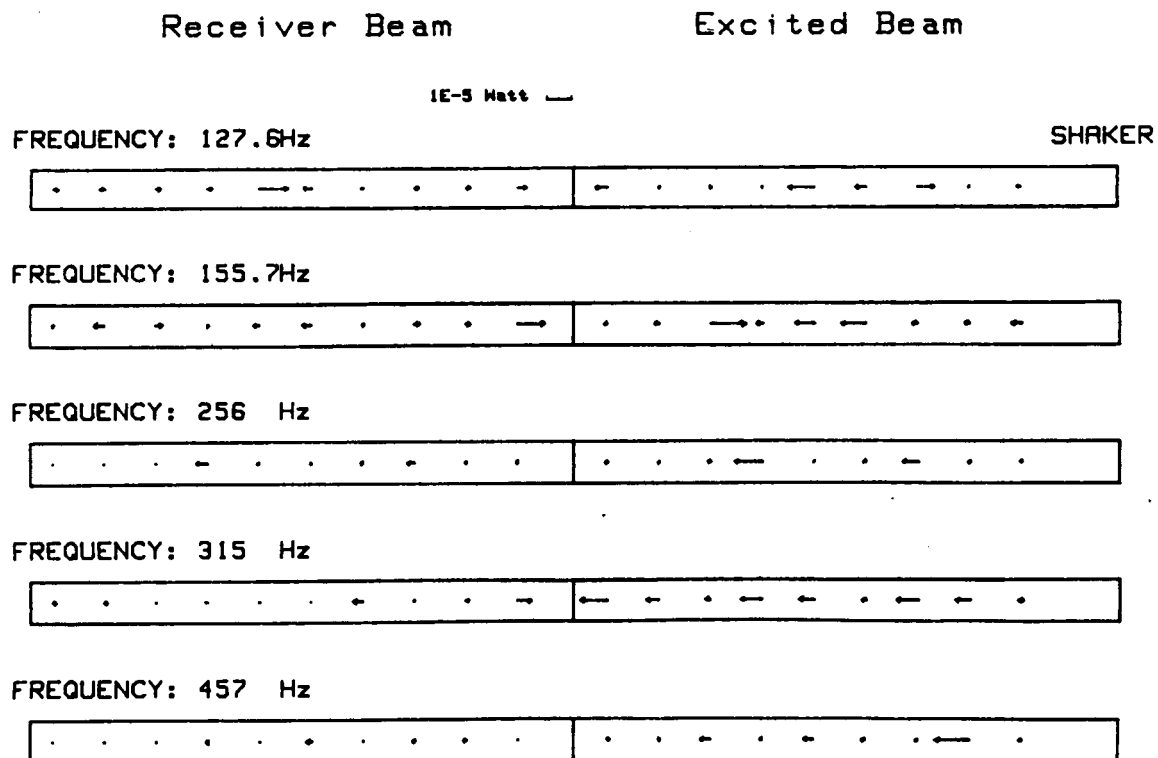


Figure 19. Time domain results for power flow in beams with an average loss factor of 0.015.

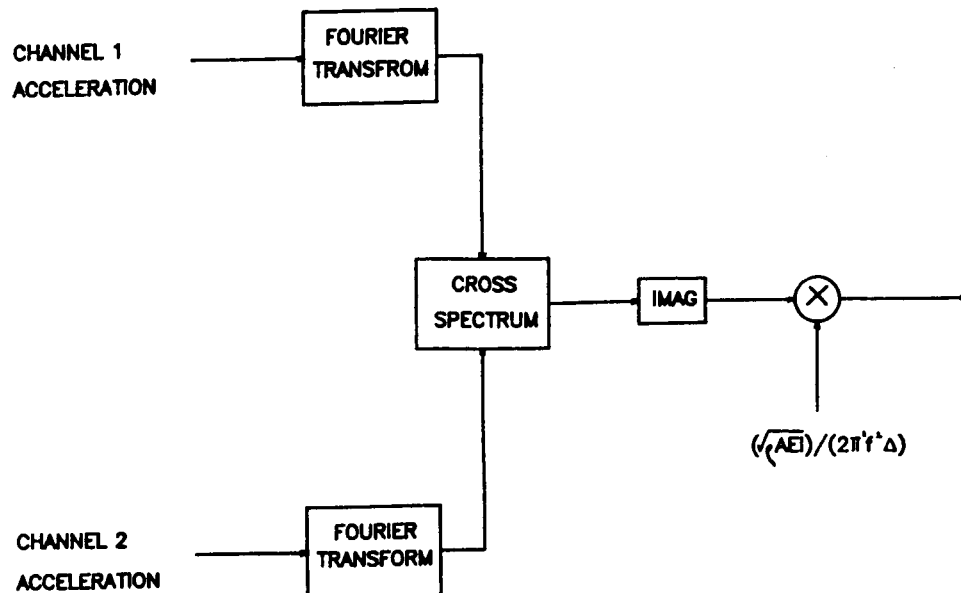


Figure 20. Processing procedure for the frequency domain measurement of power flow.

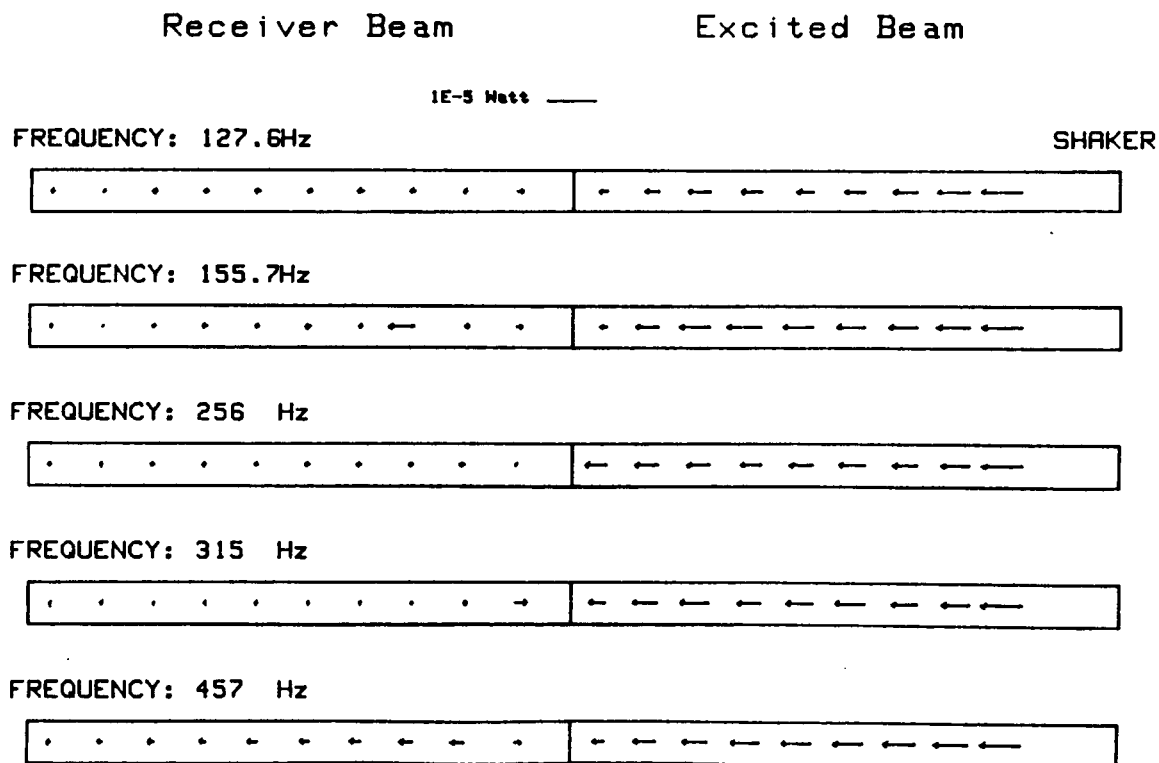
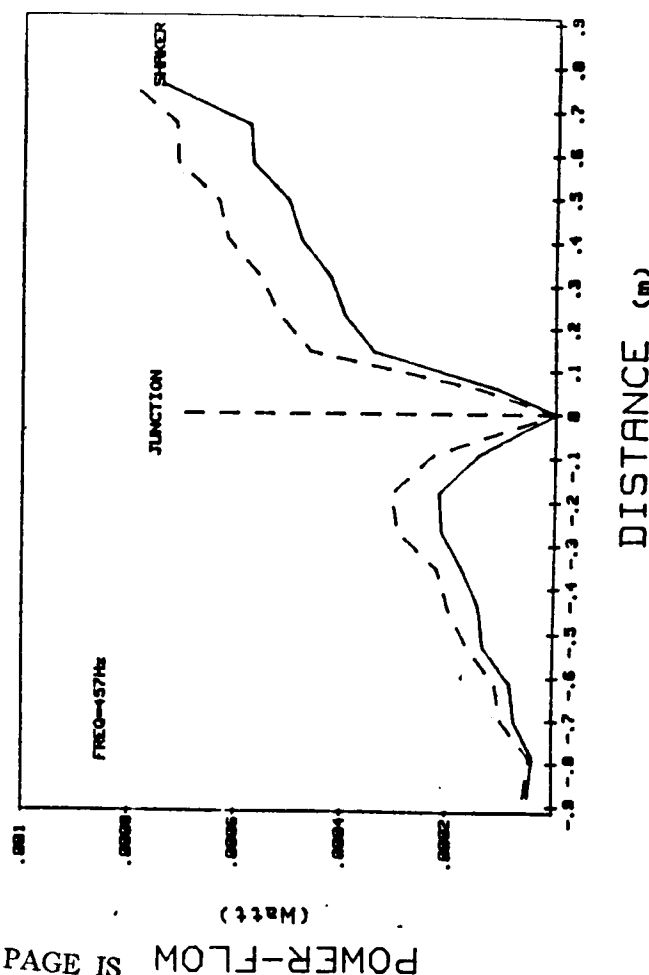
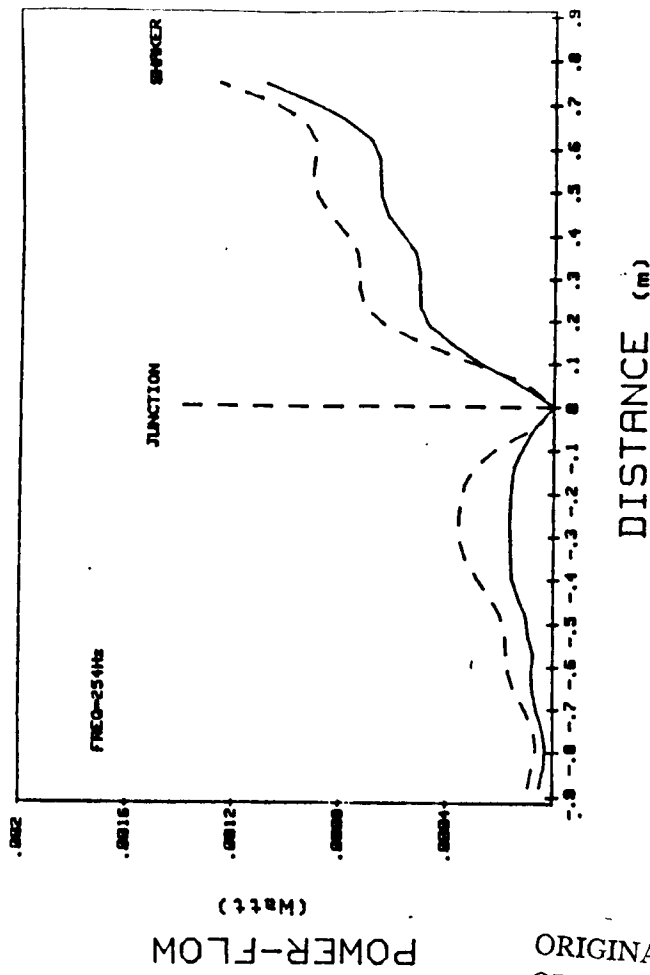
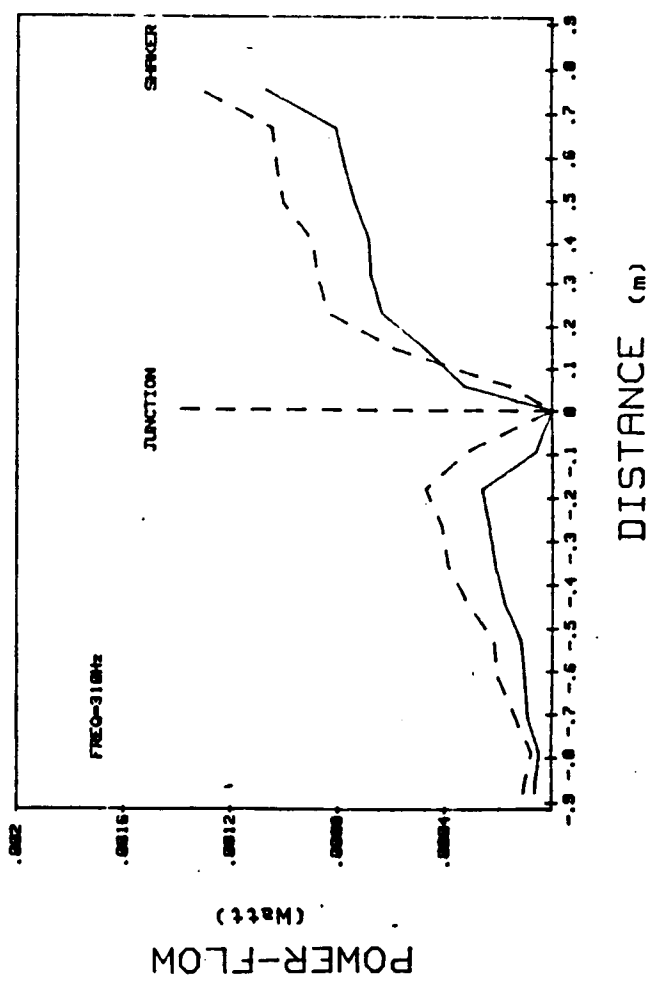
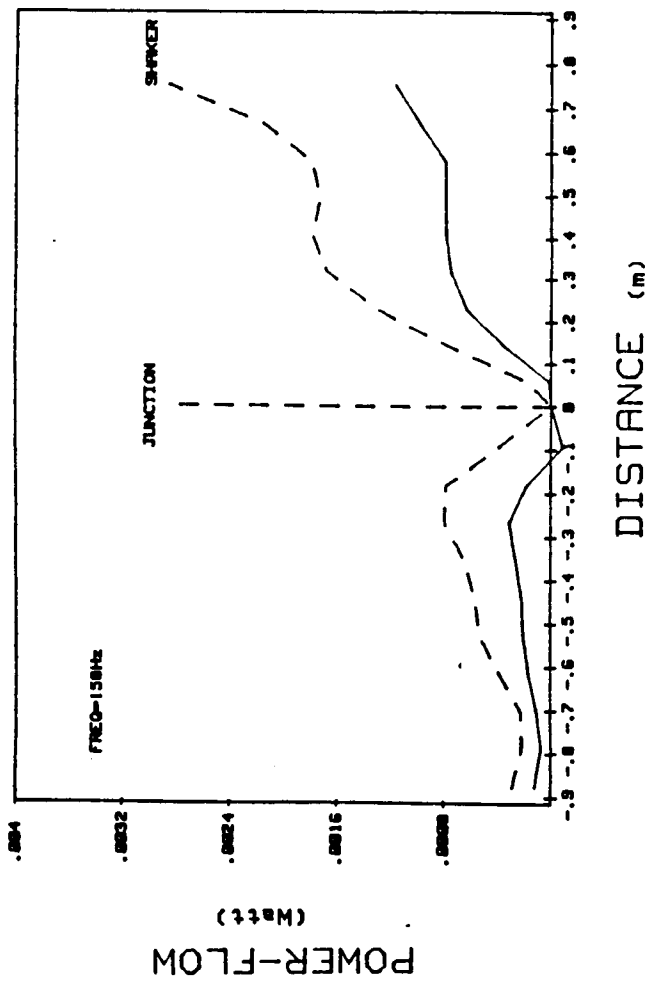


Figure 21. Power flow results using a frequency domain approach. Beams average loss factor 0.015.



ORIGINAL PAGE IS  
OF POOR QUALITY

Figure 22. Power flow in L-shaped beam, Theoretical results (---) and experimental results (—)  
Beam average loss factor 0.054.

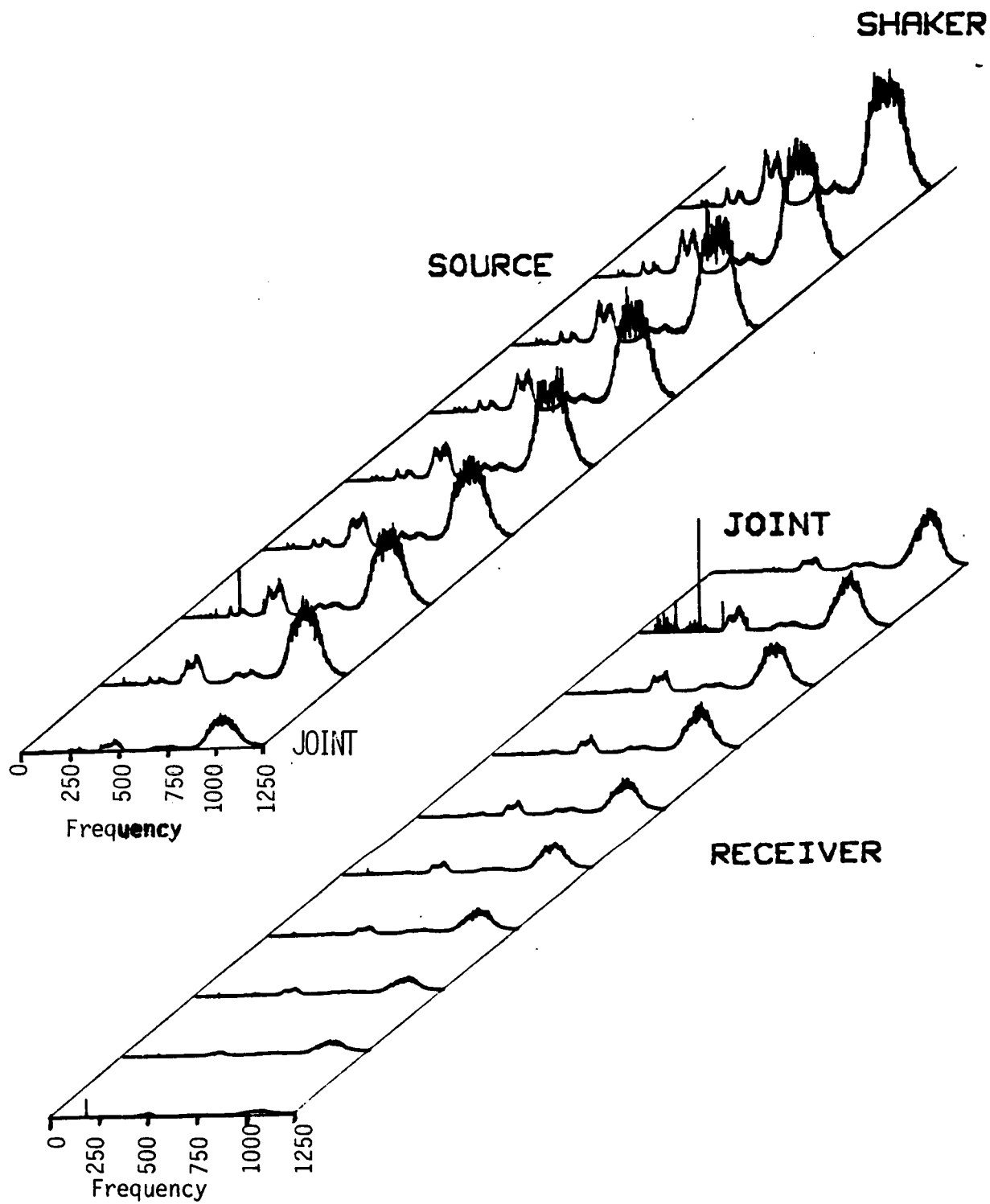


Figure 23. Broad band power flow results with beams with average loss factor of 0.054 .